Journal of Sound and Vibration (1998) **215**(3), 527–545
Article No. sv981659

NUMERICAL DIMENSION-REDUCTION METHODS FOR NON-LINEAR SHELL VIBRATIONS

S. Foale and J. M. T. Thompson

Centre for Nonlinear Dynamics, *University College London*, *Gower Street*, *London*, *WC*1*E* 6*BT*, *England*

and

F. A. McRobie

Cambridge University Engineering Department, *Trumpington Street*, *Cambridge*, *CB*2 1*PZ*, *England*

(*Received* 28 *February* 1997, *and in final form* 7 *April* 1998)

A number of methods are investigated for obtaining a low-dimensional dynamical system from a set of partial differential equations describing the non-linear vibrations of a shallow cylindrical panel under periodic axial forcing. In these approaches an initial (high-dimensional) spatial discretization of a (possibly irregular) domain is performed and a subsequent procedure is used to further reduce the resulting set of ordinary differential equations. In particular the results suggest that a numerical method based upon inertial manifold approximation is possible, but for the specific cases studied, no advantage could be discerned over more direct dimension-reduction techniques.

1. INTRODUCTION

The problem is addressed of finding the appropriate mathematical method with which to analyze the non-linear vibrations of structures of irregular shape. Obviously for irregular domains, spatial discretization by using finite-element or finite-difference models is routine but to study the non-linear vibrations of these, the analyst is faced with a model of very high dimension. The question is therefore: what methods can be used to reduce the dimension of such models which still retain the essential features of the non-linear dynamics?

For regular domains the linear vibration modes are usually well-known and provide a suitable basis for further analysis of non-linear effects. As exemplified by papers such as those of Holmes and Marsden [1] and Baumgarten *et al*. [2], a common approach is to keep only the first few vibration modes (or some similar set of *global* basis functions described by known, closed-form, analytical expressions) and to obtain a low-dimensional dynamical system governed by a few ordinary differential equations (ODEs) by using a Galerkin projection of the full partial differential equation (PDE) onto the subspace spanned by these few functions. Standard analytical and numerical techniques of non-linear dynamical systems theory can then be used manageably to study the bifurcational behaviour of the (low-dimensional) set of ODEs which approximately describe the behaviour of the original system. This procedure presumes that the functions onto which the PDE is projected are sufficient to capture the important features of the infinite-dimensional dynamical system. An *ad hoc* way of checking whether the essential features are captured is to increase the number of modes (or basis functions) until some

0022–460X/98/330527 + 19 $30.00/0

sort of convergence is achieved. This can be a fairly work-intensive process. It is a relatively simple procedure in a linear statics problem with a unique equilibrium solution: but in a non-linear dynamical system with multiple steady states which bifurcate as a parameter is changed, it is much more difficult to establish whether convergence has taken place. It would require, for example, that the bifurcation structures of different dimensional ODEs be the same, or at least very similar.

Holmes and Marsden [1] presented more rigorous arguments, based on centre manifold theory, to justify a finite-dimensional approximation in a panel flutter problem, at least for bifurcations of the fixed point at the origin. More recent work on low-dimensional behaviour in PDEs has used the concept of an *inertial manifold*, which is a finite-dimensional, positively-invariant, exponentially- and globally-attracting submanifold of the phase space. If an inertial manifold exists and can be found for a particular system then investigating the dynamics is reduced to a finite-dimensional, and therefore tractable, problem. Practical methods have been proposed for the computation of approximate inertial manifolds: see, for example, references [3, 4]. These are based on the usual Galerkin projection method for modal discretization of a PDE. A two-level projection is attempted in which the modes are split into "active" and "passive" modes. The passive modes are assumed to be slaved to the active ones and the inertial manifold describes the form of this slaving. Looked at in this way, the procedure can be seen as a way of correcting the straight-forward Galerkin projection, and has thus acquired the name *non-linear Galerkin method*.

The aim here is to investigate the application of such a two-level projection to a particular shell model. However, conscious of the need for methods that are suited to domains of irregular shape, finite differences for the initial spatial discretization are employed, rather than a decomposition onto a set of analytic global basis functions. The general approach described here can readily be extended to other spatial discretization methods.

The model adopted as an example in the following sections is essentially the shell panel studied by Baumgarten *et al*. [2]. It has a regular geometrical shape, allowing Baumgarten *et al*. to employ global basis functions with results that can be used for comparison. Obviously, the finite difference approach does not depend upon the regularity of the domain.

2. THE MODEL

The example model describes the large deflections of a shallow cylindrical panel under periodic axial loading, as illustrated in Figure 1. The equations, based on Donnell's shallow shell theory, are of the form

$$\frac{D}{m}\nabla^4 w + \frac{\partial^2 w}{\partial t^2} + \frac{\beta}{m}\frac{\partial w}{\partial t} + \frac{\beta_2}{m}\frac{\partial}{\partial t}\nabla^4 w$$

$$= \frac{1}{m}\left(\frac{1}{R}\frac{\partial^2 \Phi}{\partial x^2} + \frac{\partial^2 \Phi}{\partial y^2}\frac{\partial^2 w}{\partial x^2} - 2\frac{\partial^2 \Phi}{\partial x \partial y}\frac{\partial^2 w}{\partial x \partial y} + \frac{\partial^2 \Phi}{\partial x^2}\frac{\partial^2 w}{\partial y^2}\right), \tag{1}$$

$$\frac{1}{Eh}\nabla^4 \Phi = -\frac{1}{R}\frac{\partial^2 w}{\partial x^2} + \left(\frac{\partial^2 w}{\partial x \partial y}\right)^2 - \frac{\partial^2 w}{\partial x^2}\frac{\partial^2 w}{\partial y^2}. \tag{2}$$

Here, w is the normal displacement (positive inward), Φ is the in-plane Airy stress function and t is the time. The meridional and circumferential length co-ordinates are x and y,

respectively. The parameters are as follows: E, Young's modulus; m, the mass per unit area; β, the coefficient of proportional damping; β_2, the visco-elastic damping coefficient (see below); R, the radius of the panel; h, the thickness of the panel; a, the length of the sides of the square panel; $D = Eh^3/[12(1 - \nu^2)]$, the flexural rigidity of the panel; ν, Poisson's ratio.

In the numerical simulations, the following values have been adopted: values $E = 210 \times 10^9$ N/m^2, $m = 78{\cdot}5$ kg/m^2, $\beta = 707{\cdot}1$ Ns/m, $\beta_2 = \beta/(16\pi^4)$, $R = 8{\cdot}333$ m, $h = 0{\cdot}01$ m, $a = 1{\cdot}0$ m and $\nu = 0{\cdot}3$. In addition to equations (1) and (2), boundary conditions are imposed on the displacement w and the stress function Φ to define the problem completely. It is in the boundary conditions for the stress function that the forcing function is incorporated. The boundary conditions on the displacement, w, are that the panel is simply supported along each edge. These simplify to

$$w(x, y) = \partial^2 w/\partial x^2 = 0 \quad \text{at } x = 0 \quad \text{and } x = a,$$

$$w(x, y) = \partial^2 w/\partial y^2 = 0 \quad \text{at } y = 0 \quad \text{and } y = a. \tag{3}$$

The boundary conditions on the stress function, Φ, are

$$\partial^2 \Phi/\partial y^2 = -p(t), \quad -\frac{\partial^2 \Phi}{\partial x \partial y} = 0 \qquad \text{at } x = 0 \quad \text{and } x = a,$$

$$\partial^2 \Phi/\partial x^2 = -\partial^2 \Phi/\partial x \partial y = 0 \qquad \text{at } y = 0 \quad \text{and } y = a. \tag{4}$$

These impose a compressive stress resultant of $p(t)$ along the x (meridional) direction of the panel, where

$$p(t) = p_0 + p_1 \cos(\Omega t). \tag{5}$$

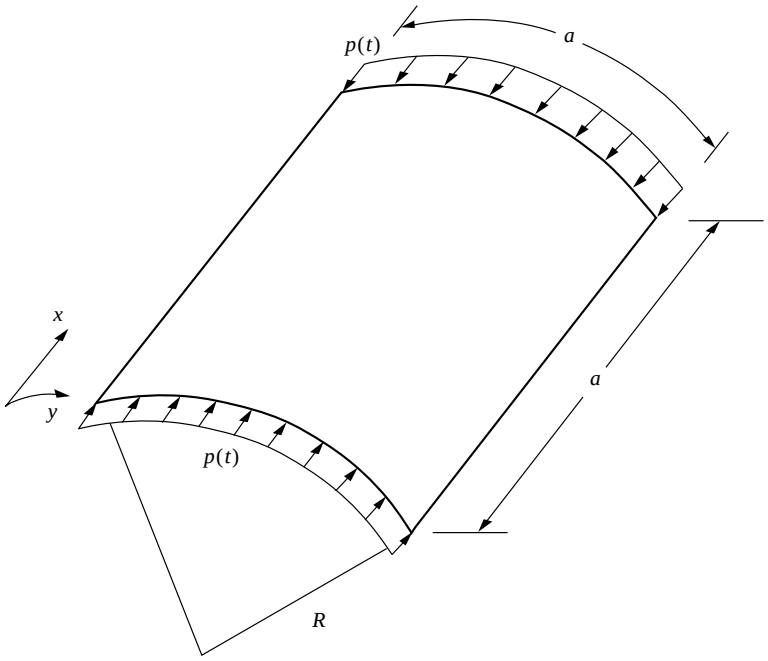

Figure 1. The shallow cylindrical panel under periodic axial loading: $p(t) = p_0 + p_1 \cos(\Omega t)$.

A conventional eigenvalue analysis of the linearised equations about the trivial solution $w(x, y) = 0$, $\Phi(x, y) = -p_0 y^2/2$, gives the static buckling loads (see for example reference [5])

$$p_{0,cr}(j, k) = \frac{D\pi^2}{a^2}\left[\frac{j^2 + k^2}{k}\right]^2 + \frac{Eh}{R^2}\frac{a^2}{\pi^2}\left[\frac{k}{j^2 + k^2}\right]^2, \tag{6}$$

with corresponding buckling eigenvectors

$$w = A \sin(j\pi x/a) \sin(k\pi y/a). \tag{7}$$

The critical buckling load for the example panel is thus $p_{0,cr}(1, 1) = 1525 \times 10^3$ N/m.

Throughout the remaining analysis the static compressive loading is kept fixed at the value $p_0 = 895 \times 10^3$ N/m, roughly 60% of the buckling load. Further linear eigenvalue analysis gives the natural frequencies as

$$\omega(j, k) = \frac{j\pi}{a}\sqrt{\frac{p_{0,cr}(j, k) - p_0}{m}}, \tag{8}$$

and for such a panel of uniform thickness, the buckling and vibration eigenvectors are coincident. For the chosen value of axial static compressive load p_0, this gives a fundamental frequency $\omega(1, 1) = 281{\cdot}4\ \mathrm{s}^{-1}$ (44·8 Hz). To follow Baumgarten *et al*. [2], we fix the excitation frequency for our studies at $\Omega = 617{\cdot}9\ \mathrm{s}^{-1}$ (98·34 Hz). This gives a ratio of forcing to natural frequencies of $\Omega/\omega = 2{\cdot}19$, putting us close to the parametric resonance condition $\Omega/\omega = 2{\cdot}0$ where one would expect the purely in-plane small vibrations to be unstable, with the panel exhibiting parametrically excited transverse vibrations. The variable parameter in this study is the amplitude of dynamic harmonic forcing p_1. At sufficiently large values of p_1 one would expect the trivial in-plane forced vibration solution to become unstable at a period-doubling bifurcation as the value of p_1 crossed the familiar V-shaped instability boundary centred around $\Omega/\omega = 2{\cdot}0$ on an Ince–Strutt diagram (with the sharpness of the V-shape rounded off by damping as usual).

The chosen value of the proportional damping coefficient β corresponds to 1·6% of critical damping. The value of the visco-elastic material damping coefficient β_2 is chosen (somewhat arbitrarily) to give a total (first mode) damping of 2% of critical. The algebra behind this follows readily from linear analysis of the damped vibrations, which have eigenvalues

$$\lambda(j, k) = (-\zeta(j, k) \pm \mathrm{i}\sqrt{1 - \zeta^2(j, k)})\omega(j, k) \qquad \text{with} \qquad \zeta\omega = \frac{\beta + \beta_2(j^2 + k^2)^2\pi^4}{2m}. \tag{9}$$

From this it can be seen that the visco-elastic damping causes the modal damping ($-\mathrm{Re}(\lambda)$) to increase for higher modes, and the relevance of this will be considered later.

3. SPATIAL DISCRETIZATION OF THE MODEL

To study the dynamical system described by equations (1)–(4) we need to use a numerical approximation method. The first step of any such approximation is to discretize spatially in some way. Galerkin projection onto global basis functions is commonly used, but as well as requiring rather regular domains, it has the further disadvantage of requiring a considerable amount of algebraic manipulation (including explicit (spatial) integrations of products of many trigonometric functions) for such a complicated set of governing equations. One approach is to use symbolic computation packages, but even that is really

practical only for a few basis functions. Baumgarten *et al*. [2] tackled the problem using such a global Galerkin approach, but the boundary conditions in the stress function cannot be satisfied exactly.

A spatial discretization by using finite difference methods is easier to implement and more generally applicable. By approximating the spatial derivatives at a grid of points by using the standard finite difference formulae, a set of second order ODEs for w is obtained which can then be integrated forwards in time directly. One can easily generate an arbitrarily large number of ODEs in this way. The number of equations generated is limited only by the amount of work one is prepared to do to integrate the resulting ODEs numerically.

3.1. THE FINITE DIFFERENCE PROCEDURE

The procedure for the initial spatial discretization is essentially standard numerical approximation. However, it is described in some detail in this section in order to establish the nomenclature ready for our subsequent developments from this basic platform.

Figure 2(a) shows the regular grid used over the panel to create the finite difference model. Additional points outside the panel allow for the imposition of the boundary conditions. The highest derivatives in the equations are associated with the biharmonic operator, ∇^4, whose finite difference approximation is given by the 13-point formula shown pictorally in Figure 2(b).

There are two stages to the finite difference spatial discretization of the coupled equations (1) and (2). First, equation (2) must be solved for the stress function Φ in terms of the current displacement w. This is a straightforward procedure since this equation is linear in Φ (given $\mathbf{w}$), so after finite difference formulae have been applied at each point of the grid, a linear (in Φ) equation is obtained:

$$\mathbf{F}\boldsymbol{\Phi} = \mathbf{g}(\mathbf{w}, t). \tag{10}$$

Here $\mathbf{F}$ is the matrix of coefficients obtained from the biharmonic operator and the derivative boundary conditions on Φ, $\boldsymbol{\Phi}$ is the vector (Φ_I, Φ_B) of values of the stress function at each internal (I) and boundary (B) grid point, and $\mathbf{g}(\mathbf{w}, t)$ is the vector given by the right side of equation (2) and the boundary conditions, equation (4).

The regular grid of Figure 2 has spacing h in either direction, and the fineness of the grid is conveniently specified by $n = a/h$. The grid also extends one point outside the physical area of the cylindrical panel with so-called "ghost points" (open circles) which allow the same finite difference formulae to be used at each internal grid point (solid circles). Equation (10) describes a linear relationship between the internal points and boundary points (crosses). There are $(n-1)^2$ equations from applying the biharmonic operator at each internal point and an additional $4(n+1)$ equations included to account for the boundary conditions (two at each boundary point). This gives a total set of $n^2 + 2n + 5$ equations. The total number of grid points (internal, external and boundary) is $n^2 + 6n + 9$. Thus, there are more grid points than equations. This anomaly can be overcome by applying appropriate difference formulae at the four corners so as to avoid the appearance of the extreme corner points. When using these formulae there are then the same number of equations as unknowns.

It should be noted here that since the boundary conditions on Φ are all in the form of second derivatives, then in the computed Φ there will be an arbitrary constant, and arbitrary slopes in the x and y directions. This arbitrariness will be apparent in the matrix $\mathbf{F}$ which will be singular, with a rank deficiency of 4. This matrix $\mathbf{F}$ can be inverted using the usual pseudo-inverse method based on the singular value decomposition (for details see reference [6]). Since only the second derivatives of Φ are used in equation (1) this

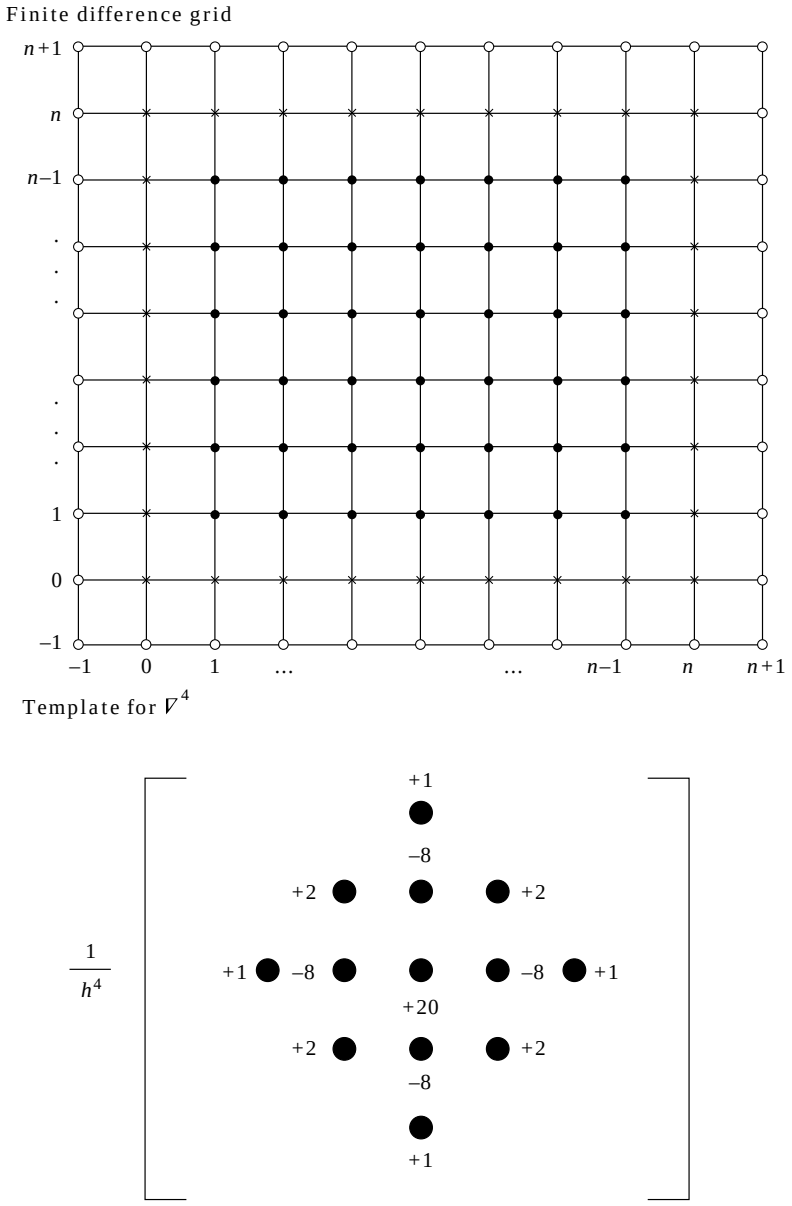

Figure 2. The upper diagram shows the finite difference grid used to cover the cylindrical panel. The lower diagram illustrates the 13-point finite difference formula for the biharmonic operator.

arbitrariness is not important. Note that despite the computationally expensive nature of the pseudo-inverse procedure, this needs to be performed only once, since the matrix **F** always remains the same.

Once the values of Φ have been calculated at each internal grid point, the information required for the discretization of equation (1) is available. The boundary conditions, given by equation (3), on the displacement w are easier to impose than those for the stress function. The boundary points all have a displacement of zero, and the second derivative in the direction normal to each edge is zero. This implies that the values taken at the ghost

points are simply the negative of the adjacent internal points. The finite difference procedure can therefore be applied directly to each internal grid point for equation (1). This will result in $2(n-1)^2$ second order ODEs, one for each w_i, the displacement at each internal grid point.

In order to accord with the mathematical literature which deals with first-order differential equations of the form

$$\dot{\mathbf{x}} = \mathbf{A}\mathbf{x}, \tag{11}$$

rather than the usual second-order equation of structural elastodynamics

$$\mathbf{m}\ddot{\mathbf{x}} + \mathbf{c}\dot{\mathbf{x}} + \mathbf{k}\mathbf{x} = \mathbf{f}, \tag{12}$$

the usual procedure is adopted for replacing each second-order ODE by two first-order ODEs by letting $u_{2i-1} = w_i$ and $u_{2i} = \dot{w}_i$. (This leads to a slight difference of nomenclature for the eigenvectors and eigenvalues. In the standard structural dynamics usage, the eigenvectors are usually the free vibration mode shapes with associated algebraic eigenvalues ω_j^2, where ω_j are the undamped natural frequencies. In the mathematical description, the eigenvectors describe both modal displacements and velocities, and the eigenvalues are complex and include the effects of damping).

One thus obtains an expression of the form

$$\dot{\mathbf{u}} = \mathbf{G}(\mathbf{u}, t), \tag{13}$$

where $\mathbf{u}$ is the vector of all of the transverse displacements and velocities and $\mathbf{G}$ is the function obtained by the finite difference procedure. This set of equations can be numerically integrated, in the usual way, in order to explore the dynamical behaviour of the approximated system. However, the size of the problem grows rapidly as n, which controls the size of the grid, increases. Because of this problem of high dimensionality, resulting from the finite difference spatial discretization, we explore in section 4 the possibility of tackling the problem using dimension-reducing techniques. First, for reasonably small n, we present some results from direct numerical integration.

3.2. INTEGRATION OF THE FINITE DIFFERENCE SHELL MODEL

For moderately-sized grids, it is feasible to numerically integrate the set of equations obtained from the finite difference discretization. Using the shell model of section 2 and putting $n = 6$, one obtains a set of 50 first order ODEs describing the time evolution of w and $\dot{w}$. Like most equations of structural dynamics, these ODEs are very stiff. However, rather than adopting any of the more traditional methods of structural dynamic analysis, such as the Newmark β or Hilber—Hughes–Taylor algorithms, we elected to use a standard stiff integrator from the numerical analysis literature: a Rosenbrock method (see e.g., reference [7]).

Although it would have been possible to apply numerical path-continuation methods to the system of ODEs, such effort was felt to be unnecessary, since only a skeletal description of the bifurcation structure is needed at this stage. (Indeed, the effort that such a task would require is a major reason for looking at low-dimensional modelling techniques.) The bifurcation diagram shown in Figure 3 was thus obtained by direct time-integration, slowly ramping the magnitude of harmonic forcing p_1. Obviously, only stable solutions can be obtained by this method. Various initial conditions were chosen in order to locate coexisting solutions. The displacement of the centre of panel (u_{25}) at an arbitrarily-chosen Poincaré (stroboscopic) section is plotted against p_1.

The bifurcation pattern that emerges is quite complex, and thus we include a simple schematic sketch of the basic structures in Figure 4(a) as an aid to understanding. Starting

from the trivial $w = 0$ solution at $p_1 = 0$, a stable path with zero out-of-plane amplitude emerges. At a value of $p_1 \approx 250 \times 10^3$ N/m, this trivial solution undergoes its first period-doubling bifurcation. (This is the value at which the parameter sweep crosses the V-shaped Ince–Strutt instability boundary.) Unfortunately, the non-zero lateral displacements of the period-doubled solution are so small at the chosen Poincaré section that this bifurcation is not discernible on the main small-amplitude path running through Figure 3. Further increases of p_1 lead to further bifurcations of the transverse oscillations, again sketched in Figure 4(a) but not visible in Figure 3.

Also present at $p_1 = 0$ is a stable large-amplitude, buckled solution (with $u_{25} \approx 0{\cdot}025$ m). A schematic of the static buckling behaviour is sketched in Figure 4(b). (At the chosen value of static load p_0 one thus also anticipates an unstable buckled configuration (B) to exist between the trivial unbuckled (A) and stable buckled (C) states.) As the harmonic forcing p_1 is increased from zero, the structure exhibits small, directly-forced oscillations about the large-amplitude buckled configuration (C). Further increases of p_1 cause these oscillations to bifurcate in some complex manner, whose exact details do not overly concern us.

Another set of transverse oscillations exist which may be loosely described as cross-well motions or snap-through oscillations. These are denoted (D) in Figures 3 and 4(c). These are large period-two solutions whose motions extend either side of the small-amplitude oscillations around the unbuckled and buckled positions in the course of a single oscillation cycle. They do not exist in the static case and are born at a saddle-node bifurcation near $p_1 = 50 \times 10^3$ N/m. Again, for larger values of p_1 these appear to undergo bifurcation cascades leading to apparently chaotic motions.

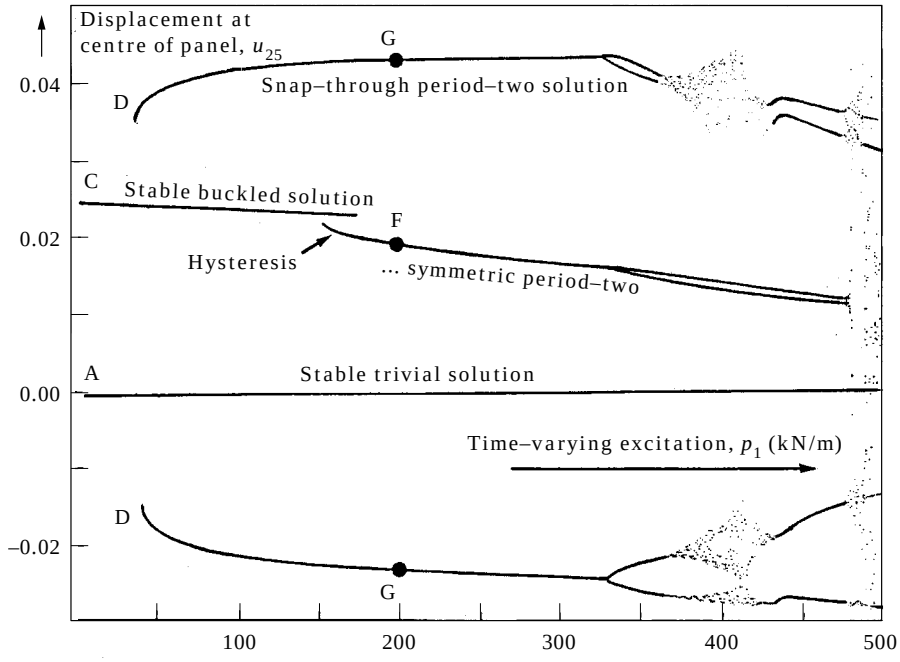

Figure 3. The bifurcation diagram obtained by direct time-integration of the set of 50 first-order ODEs generated from a finite difference grid of size $n = 6$.

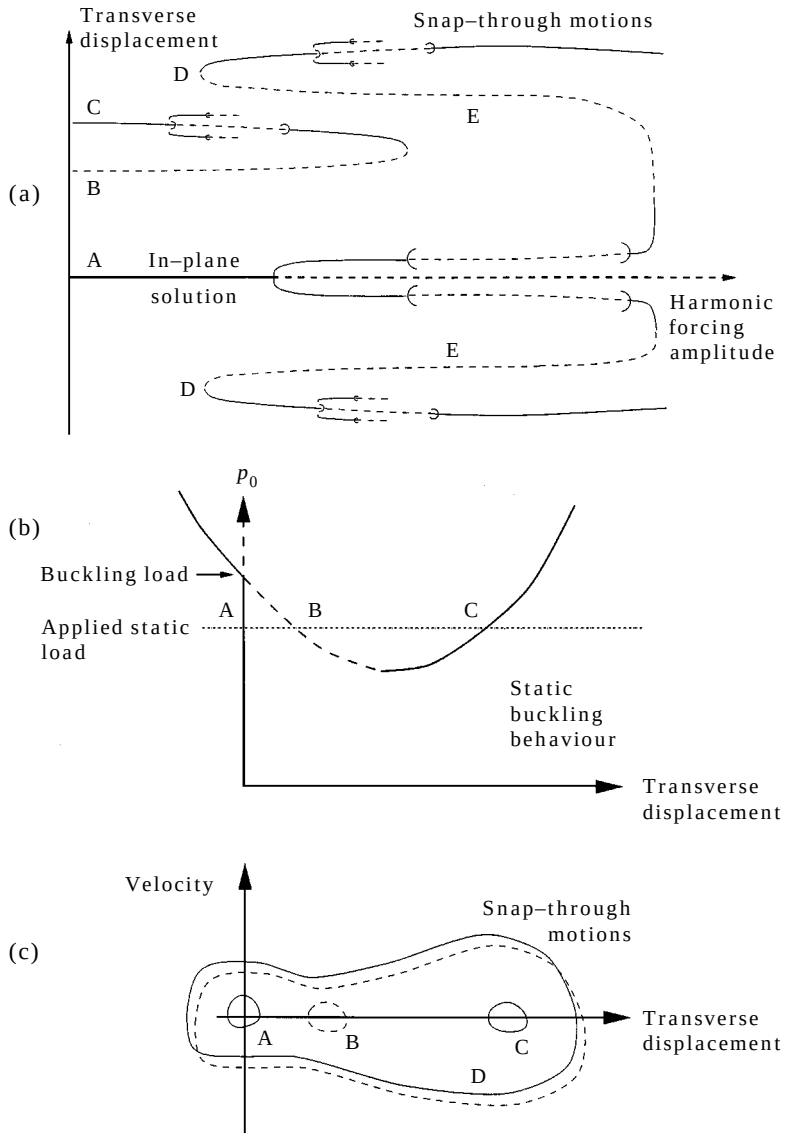

Figure 4. Schematic sketches of the major features of (a) the bifurcation diagram under increasing harmonic forcing amplitude, (b) the static buckling behaviour and (c) trajectories of significant orbits on the phase plane.

For values of p_1 very much larger than shown, a number of the early orbits appear to collide and annihilate at saddle-node bifurcations, as sketched in Figure 4(a). In particular, the small oscillations around the unstable (B) and stable (C) buckled solutions appear to collide, as do the large unstable period-two snap-through orbits (E) with the path emerging from the initial Mathieu period-doubling from the trivial path (A).

The displacement fields for two of the oscillations are illustrated in Figure 5. Figure 5(a) corresponds to point F, Figure 3, and illustrates a small (period 2) oscillation about the buckled state (C). Figure 5(b) shows a large amplitude period 2 snap-through oscillation (corresponding to point G, Figure 3).

4. STRATEGIES FOR DIMENSION REDUCTION

The method described above for integrating the shell model uses standard numerical procedures, but requires the forward time-integration of a set of equations of rather high dimension. To investigate in detail the response of a complex dynamical system such as the one described here, direct integration is often inadequate. For example, it is often desirable to follow the path of a fundamental solution and identify rigorously the bifurcations which it undergoes and to locate and follow the paths of unstable periodic

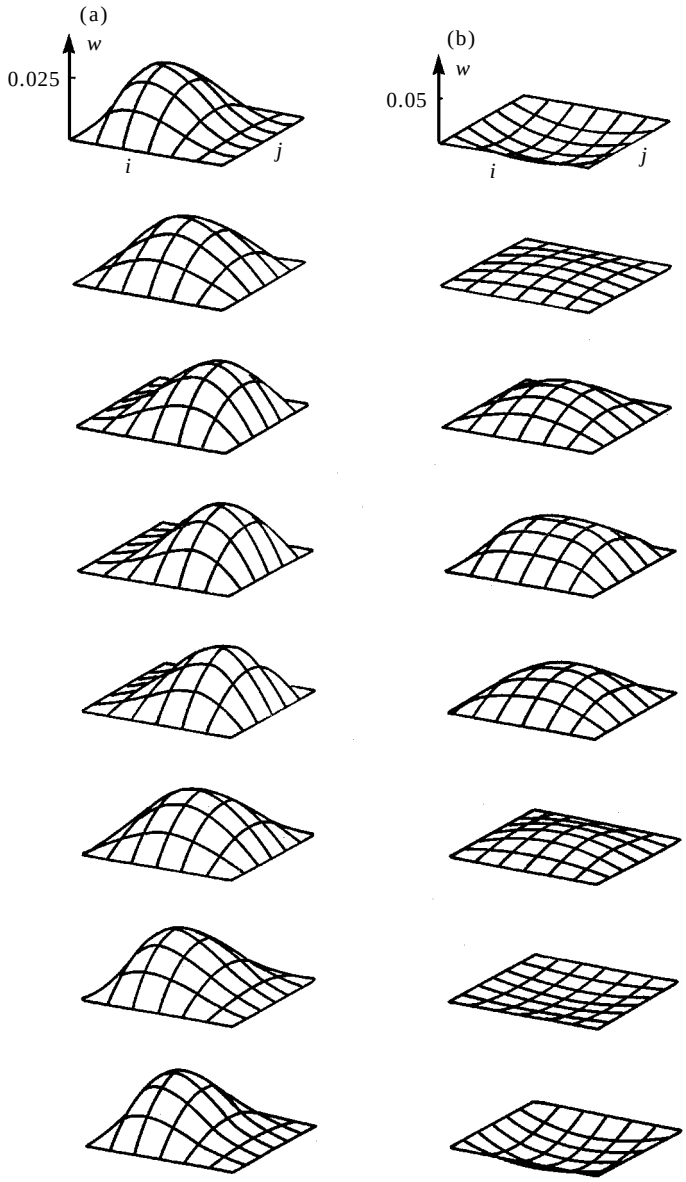

Figure 5. Two sample oscillations corresponding to points F and G of Figure 3, at $p_1 = 200 \times 10^3$ N/m, showing the displacement field, w, at eight equally spaced time intervals throughout two periods of the forcing; $0 < t < 4\pi/\omega$. (a) A symmetric period-two motion about the buckled state. (b) A large-amplitude snap-through motion which buckles inwards and outwards with period 2.

orbits by using path continuation methods. For high-dimensional systems like the one obtained above, the work required to perform such tasks can be prohibitive. A low-dimensional model may also be useful for quickly scanning large expanses of parameter space for unstable or important phenomena which may then be studied in more detail by a more realistic model.

If Galerkin's method is used to project the governing equations onto just a few global basis functions, then after some considerable algebraic effort, a low-dimensional dynamical system can be produced which is amenable to full investigation. However, such an approach implicitly assumes that the modes (or global basis functions) onto which the Galerkin projection is made are the important ones and that the effects of the remaining modes can be ignored.

To obtain a low-dimensional dynamical system using the finite difference approach one could simply use an extremely coarse grid, but one would not expect this to lead to a good approximation of the dynamics. We have two conflicting requirements then. On the one hand, we would like to be able to use *local* spatial discretizations, such as finite differences, because they are easy to implement and applicable to irregular domains. On the other hand, the use of *global* basis functions offers the possibility of a low-dimensional description which may be capable of capturing the essential dynamics.

Recently, there has been much interest in methods of reducing the dimension of dynamical systems using the ideas of approximate inertial manifolds, employing an approach known as the non-linear Galerkin method. To summarize this approach, first we assume that we are given a PDE.

$$\dot{u} = Au + F(u), \tag{14}$$

where A is a dissipative, linear operator and F is the remaining, non-linear operator. Usually there is a further assumption that the eigenfunctions of A form an orthogonal basis $\{w_i\}$ such that $Aw_i = \lambda_i w_i$, with spectrum $\mathrm{Re}\,(\lambda_1) > \mathrm{Re}\,(\lambda_2) > \cdots > \mathrm{Re}\,(\lambda_n) > \cdots$, such that $\mathrm{Re}\,(\lambda_n) \to -\infty$ as $n \to \infty$. With the projection onto the span of the first m eigenvectors denoted by P and the projection onto the remaining eigenvectors denoted by Q one can rewrite equation (14) as the coupled set of equations

$$\dot{p} = Ap + PF(p + q), \qquad \dot{q} = Aq + QF(p + q), \tag{15}$$

where $p = Pu$ and $q = Qu$ is the decomposition of u into the two subspaces.

If one makes the assumption that an inertial manifold exists, one can assert the existence of a function Ψ such that $q = \Psi(p)$. This function defines how the behaviour of the higher modes q is completely slaved to the lower modes p. For appropriate choices of the basis functions and of m, (the number of the mode at which one splits u into p and q) this can be shown to be a valid assumption in certain problems. One may then write the first equation in (15) with full generality as

$$\dot{p} = Ap + PF(p + \Psi(p)). \tag{16}$$

This is a set of m ODEs. If one sets $\Psi(p) = 0$ one obtains the standard Galerkin projection discussed above which is routinely used to truncate PDEs to a low-dimensional set of ODEs. This can thus be seen as a crude first guess of the inertial manifold (if indeed one exists) which may subsequently be corrected using various techniques outlined for example by Debussche and Marion [8], and Russel *et al*. [4].

In order to go beyond that method to use the non-linear Galerkin method, one needs to know the function Ψ. To find this explicitly can be extremely difficult, but an estimate of it may be obtained from the second of equations (15). Upon inserting the estimate for $\Psi(p)$ into equation (16), this m-dimensional set of ODEs should give a better description

of the evolution of p than the simple Galerkin truncation. A method of estimating $\Psi(p)$ is described in section 4.3.

The essential requirement for showing the existence of an inertial manifold is the presence of a spectral gap: i.e., there must be a condition that $-\mathrm{Re}\,(\lambda_k) \ll -\mathrm{Re}\,(\lambda_{k+1})$ for some k. If it can be shown that the linear contraction from A for the higher modes dominates over any expansion in the non-linear operator F, the low-dimensional description represented by equation (16) will be sufficient. We consider the existence of such a gap for the problem at hand in the following section.

4.1. A TWO-LEVEL APPROXIMATION FOR THE FINITE DIFFERENCE DISCRETIZATION

In this section, it is shown how the essential ideas of non-linear Galerkin methods (based on the usual global Galerkin projection onto eigenmodes of a linear operator) may be adapted to apply, under certain conditions, to the alternative spatial discretization using finite differences. After the finite difference discretization of a shell model, we saw in section 3.1 that a (high-dimensional) set of ODEs, equation (13), was obtained. This equation could be rewritten as (cf. equation (14))

$$\dot{u} = Au + F(u), \tag{17}$$

where in this case A is the linear (matrix) operator obtained from the finite difference discretization of the linear part of the original PDE for w (equation (1)) and F is the remaining non-linear part arising from the non-linear part of equation (1) after having solved equation (2) for Φ in terms of w. The linear part, A, consists of the matrices arising from the finite difference discretization of the biharmonic operator and the linear and visco-elastic damping terms. This is a simple matrix to compute for various values of the grid size.

The essential characteristic that must be satisfied if the linear operator is to be dissipative is that the real parts of all eigenvalues must be less than zero. Similarly, for a spectral gap condition to hold one requires that there is a large enough gap in the real parts of the spectrum of A. Figure 6 shows the spectrum of the operator A, based upon numerical investigation of the finite difference model with a grid of size $n = 6$. Also shown is the spectrum (as given by equation (9)) based upon simple linear analysis of the governing PDEs about the trivial solution. Quantitative numerical discrepancies between the finite difference and the explicit results may be due to errors in the approximation of high derivatives by the finite difference procedure, but both are in qualitative agreement about the form of the spectrum.

Clearly all eigenvalues have negative real parts as required. Note however that in this problem it is the inclusion of the visco-elastic material damping that brings the possibility of a spectral gap. If only proportional damping is included the spectrum is flat, all modes being damped equally and no gap can exist. By including the material damping, higher modes experience higher damping and thus for high enough mode number, a spectral gap will exist, although there is no evident "large" gap over the mode numbers shown. To answer exactly how large a spectral gap is needed rests upon proving whether or not the linear contraction for the higher modes dominates over any expansion in the non-linear part of the equation and this involves considerable analytical effort for non-trivial PDEs such as the ones of this model, and we do not attempt any such rigorous analysis here.

4.2. GALERKIN PROJECTION OF THE FINITE DIFFERENCE MODEL

The simplest form of a two-level procedure for reducing dimension is, as discussed above, the ordinary or "flat" Galerkin projection in which the higher modes are set to zero. By looking at the procedure for reducing a PDE, we develop the analogous procedure for

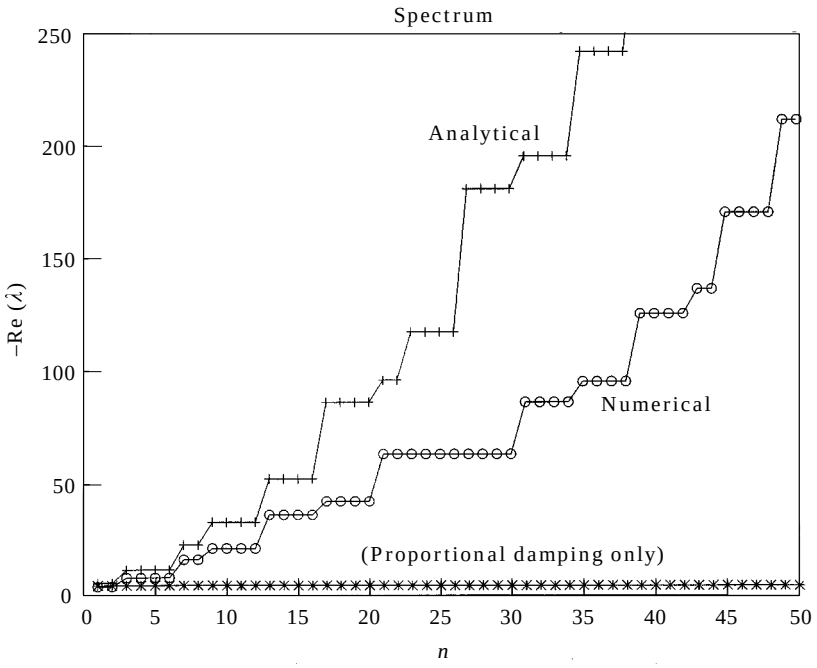

Figure 6. The real part of the eigenvaue spectrum for small oscillations about the trivial solution. Modes are ranked by frequency along the abscissa. (There is a multiplicity of two for each vibration mode caused by writing the generalised eigenvalue problem of the second-order differential equations in standard first-order form). The analytical results are obtained from equation (9). The numerical results are obtained from the matrix for the $n = 6$ finite difference grid. Also shown is the spectrum that would result if visco-elastic damping were not included.

the reduction of the large set of ODEs produced by finite differences. If a PDE can be written in the form of equation (14) and the eigenfunctions of A are all real and orthogonal, then the Galerkin projection onto the first m eigenfunctions of the linear operator A gives a lower dimensional approximation to the original equation in the form of a set of real ODEs. If the eigenfunctions of A are ϕ_i then one can write u in terms of this basis as

$$u(\mathbf{x}, t) = \sum_{j=1}^{\infty} a_j(t)\phi_j(\mathbf{x}), \tag{18}$$

where $\mathbf{x} = \{x, y\}$ is the space variable and t is time. Using a Galerkin projection we select a finite m and then take suitable inner products of equation (17) with each ϕ_i, $(i = 1, 2, \ldots, m)$ in turn. This gives the set of m ODEs

$$\dot{a}_j\langle\phi_j, \phi_i\rangle = a_j\langle A\phi_j, \phi_i\rangle + \left\langle F\left(\sum a_j\phi_j\right), \phi_i\right\rangle, \qquad i = 1, 2, \ldots, m. \tag{19}$$

Here we are concerned instead with the case of a large set of ODEs, equation (17), where the linear operator A is just a matrix ($N \times N$, say), rather than an infinite-dimensional operator. Essentially the same procedure can be carried out in this case. Instead of finding the eigenfunctions of a linear differential operator, one now needs to find the N eigenvectors of a matrix. These eigenvectors give the mode shapes in terms of u_i, the vectors of transverse displacement and velocity of the panel at each node point on its surface. From

the convenient *local* space discretization one thus obtains the *global* (numerical) mode shapes for further use.

A complication which arises is that the eigenvectors of the matrix need be neither real nor orthogonal in general. If one simply proceeds with a Galerkin projection onto a complex basis, the result would be a complex set of ODEs. Since it is more convenient to deal with real ODEs, the first step in the procedure is to form a new real basis which spans the same space as the complex one. The eigenvectors of A are all complex conjugate pairs of the form

$$(v_R + \mathrm{i}v_I)_k, (v_R - \mathrm{i}v_I)_k. \tag{20}$$

A new real basis in which each pair of real vectors (w_{2k-1}, w_{2k}) spans the subspace spanned by one of the complex conjugate pairs of eigenvectors is given by

$$w_{2k-1} = (v_R + v_I)_k, w_{2k} = (v_R - v_I)_k, \tag{21}$$

and one additionally defines the matrix W to be the matrix whose columns are the vectors w_i. Note that $W^{-1}AW$ is here a block diagonal matrix with blocks of size 2 rather than a diagonal matrix of eigenvalues.

As in the conventional Galerkin method discussed above, the first step in the procedure is to write the solution u in terms of the new basis w_i. This is just a change of variables which one can write in matrix form as

$$u = Wr, \tag{22}$$

where r is the new set of (time-dependent) variables. Next one can split the problem into low and high (or slowly- and quickly-contracting) modes, based upon the real part of their eigenvalues. One orders the basis w_i so that the first m columns arise from the least contracting eigenvectors and the remaining columns arise from the most contracting. Then one can split the new variable r as, $r = (p|q)$. Similarly one can split the matrix W into the first m columns W_p, and the remaining columns W_q, so that $W = (W_p/W_q)$. One can then write

$$u = (W_p/W_q)\begin{pmatrix} p \\ q \end{pmatrix} = W_p p + W_q q. \tag{23}$$

Substituting this into the original set of ODEs, equation (14), gives

$$W_p\dot{p} + W_q\dot{q} = AW_p p + AW_q q + F(W_p p + W_q q). \tag{24}$$

The mixture of $\dot{p}$ and $\dot{q}$ terms on the left side of this equation could, if the w_i were orthogonal, be separated by taking inner products with each w_i in turn, giving a new split system with one equation having only $\dot{p}$ terms on the left side and the other only $\dot{q}$ terms. To achieve the same splitting with the non-orthogonal basis one can use instead a weighted residual method, in which the basis functions are different from those with which we take the inner product. An appropriate choice in this case is to use Z_p, the matrix formed by columns which span the null space of W_q, and Z_q, the matrix formed by columns which span the null space of W_p. Taking inner products with these vectors splits the equation in the desired way:

$$\begin{aligned} Z_p^{\mathrm{T}} W_p\dot{p} &= Z_p^{\mathrm{T}} AW_p p + Z_p^{\mathrm{T}} AW_q q + Z_p^{\mathrm{T}} F(W_p p + W_q q), \\ Z_q^{\mathrm{T}} W_q\dot{q} &= Z_q^{\mathrm{T}} AW_p p + Z_q^{\mathrm{T}} AW_q q + Z_q^{\mathrm{T}} F(W_p p + W_q q). \end{aligned} \tag{25}$$

These can be rearranged to give two sets of partially-decoupled equations,

$$\dot{p} = X_{pp}p + X_{pq}q + Y_p(W_p p + W_q q),$$
$$\dot{q} = X_{qp}p + X_{qq}q + Y_q(W_p p + W_q q), \tag{26}$$

where X_{pp}, X_{pq}, X_{qp} and X_{qq} are the appropriate matrices and Y_p and Y_q are the non-linear terms obtained from a simple rearrangement of equation (25).

Having partially decoupled the large set of ODEs into a small set (the $\dot{p}$ equations) and a large set (the $\dot{q}$ equations) the simplest approximation one can make is to set the most contracting modes to zero: i.e., $q = 0$. This results in a small set of ODEs describing the time evolution of the least contracting modes:

$$\dot{p} = X_{pp}p + Y_p(W_p p). \tag{27}$$

As an example of this simplest two-level splitting of a finite difference approximation, our shell model is again considered, with $n = 6$. Recall that, after the initial space discretization, this gave a set of 50 ODEs, the direct integration of which was shown in Figure 3. In comparison, Figure 7 shows the result of performing a severe truncation projecting onto just the first pair of modes. The results are obtained in the same way as before, with a slow parameter sweep up and down in the external forcing, p_1, plotting the displacement of the centre of the panel at the beginning of each forcing cycle. Even this severe truncation manages to capture many of the important features shown in Figure 3: for example, the creation of the large period-two snap-through motions at $p_1 \approx 50 \times 10^3$ N/m at a saddle-node bifurcation, followed by a period doubling of this solution path at around $p_1 \approx 300 \times 10^3$ N/m, and the period-two oscillations around the

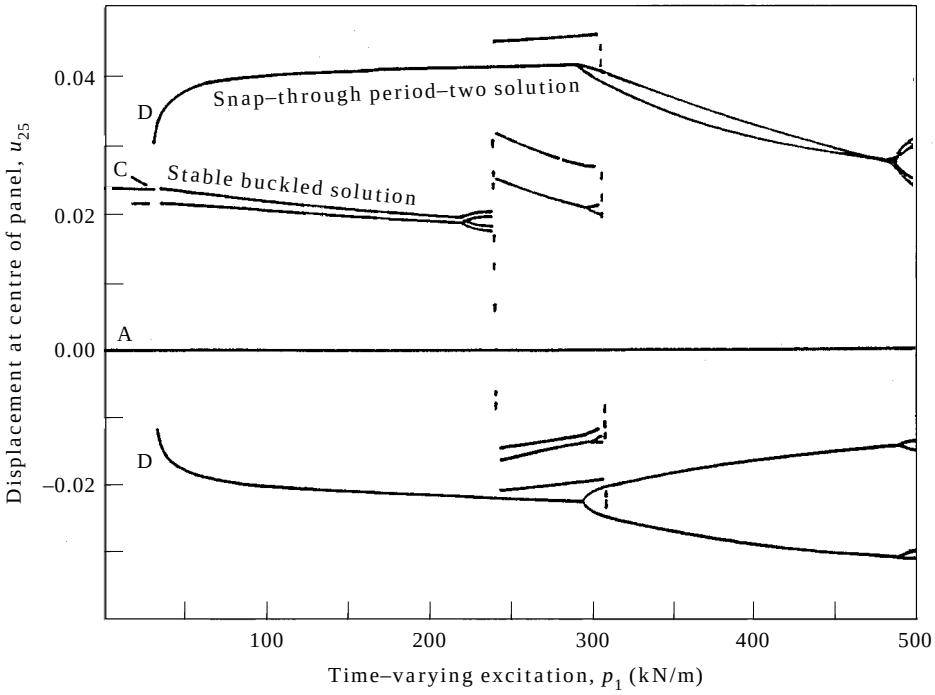

Figure 7. The bifurcation diagram for the $n = 6$ grid after a flat projection onto the first pair of modes.

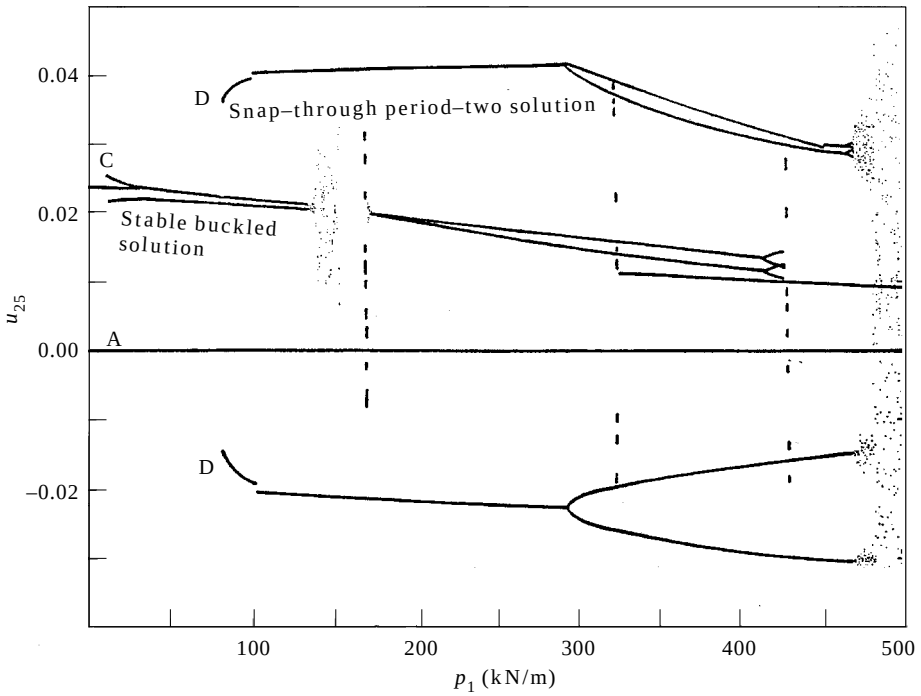

Figure 8. The bifurcation diagram from a flat projection of the $n = 6$ finite difference model onto the first three modes.

buckled state (C). In the low-dimensional approximation these latter solutions are lost at $p_1 \approx 250 \times 10^3$ N/m. It can be expected that the approximation will become worse as the non-linearity becomes larger, which will occur when the external forcing becomes large. It should be noted that not only is this two-degree-of-freedom approximation 25 times less demanding computationally than integrating the original discretization, but speed gains are also achieved due to the fact that the resulting set does not require the more costly stiff integrator.

Figure 8 shows the result of using a higher-dimensional approximation from the same discretization, this time projecting onto the space spanned by the first three pairs of complex conjugate eigenvectors of the linear operator A, giving a six-degree-of-freedom approximation. Again, the main features present in the original high-dimensional dynamical system are captured. The saddle-node bifurcation leading to the large snap-through motions is delayed until a higher value of the control p_1, but the period-doubling bifurcation along the path is again reproduced in this approximation. The period-two oscillations around a buckled position are again present, but in this case do not completely disappear as p_1 is increased.

4.3. NON-LINEAR GALERKIN SCHEME APPLIED TO THE FINITE DIFFERENCE MODEL

As discussed earlier in this section, under the assumption that the dynamical system being studied has a lower-dimensional inertial manifold, then for an appropriate two-level splitting into "low modes" p and "high modes" q there will exist a function Ψ such that $q = \Psi(p)$. As a consequence, the long-term dynamics of the system can be completely determined by the first, lower-dimensional set of ODEs with the remaining passive directions completely slaved to the active ones.

A simple method, introduced by Foias *et al*. [3] for approximating the function Ψ (upon assuming that such a function exists) is based on integrating the equation for q by using the implicit Euler method. If a suitable time step, τ say, is chosen, a contraction mapping for q results, with the fixed point of the mapping being the (invariant) inertial manifold. This procedure for constructing an approximate inertial manifold may be used with the set of equations derived by finite differences, and the subsequent two-level splitting described above, resulting in equation (26).

The first stage is to use an implicit Euler step on the least contracting modes, say with an initial condition $q_0 = 0$, which gives an approximation $\hat{q}$ to the solution at time τ:

$$\hat{q} = \tau X_{qp} p + \tau X_{qq} \hat{q} + \tau Y_q (W_p p + W_q \hat{q}). \tag{28}$$

This can be rearranged to give a mapping for q,

$$\hat{q} \rightarrowtail \tau [I - \tau X_{qq}]^{-1} (X_{qp} p + Y_q (W_p p + W_q \hat{q})), \tag{29}$$

the first iterate of which, with an initial condition of $q = 0$ (the "flat" Galerkin solution) gives an expression for Ψ:

$$\Psi_A(p) = \tau [I - \tau X_{qq}]^{-1} (X_{qp} p + Y_q (W_p p)). \tag{30}$$

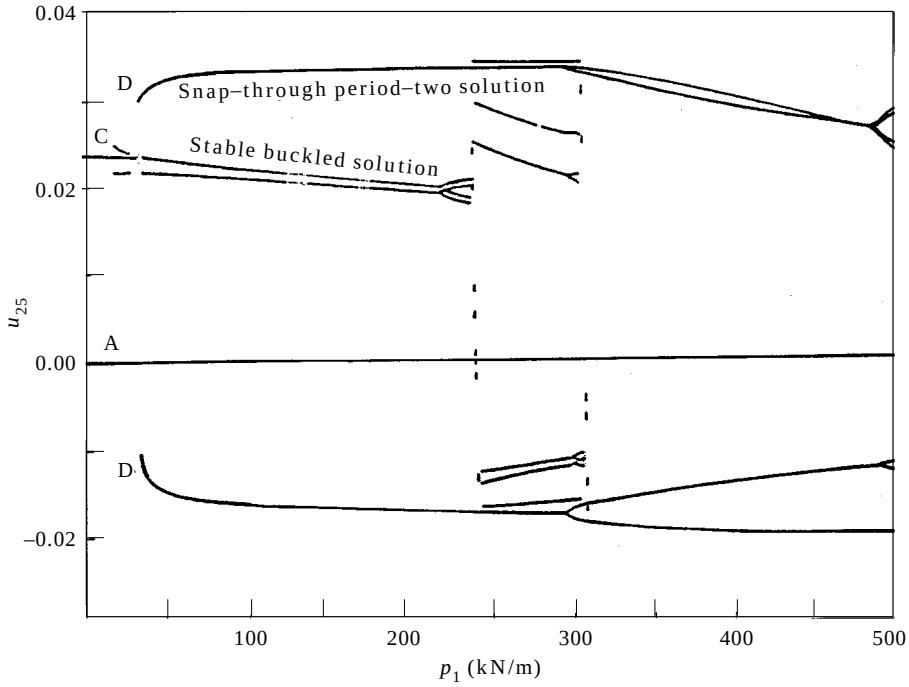

Figure 9. The bifurcation diagram obtained by using the *non-linear Galerkin procedure* to project onto the first two modes.

With this last expression for Ψ substituted into the differential equation for modes p from equation (26), one has again arrived at a set of equations, of the dimension of p, approximating the behaviour of the entire set of differential equations. Upon using a splitting, as before, with the 50 ODEs generated by the finite differences divided between the two most contracting (p) modes and the remaining 48 (q) modes, this non-linear Galerkin procedure was performed, and the resulting set of two ODEs were investigated. The resulting bifurcation diagram, Figure 9, is remarkably similar to that for the simple two-mode Galerkin truncation of Figure 7. Extra work is involved in trying to construct an approximate inertial manifold, and since the ODEs which must be numerically integrated are more complicated, the integrations are more computationally expensive. No apparent gain has been made as a result of this extra work. In this case, at least, a flat Galerkin approximation appears sufficient to reduce the dimension of a set of ODEs produced from a spatial discretization. However, it is perhaps evident from the spectrum of Figure 6 that a splitting after mode two does not correspond to a spectral gap and further work comparing the flat and non-linear Galerkin methods at higher level splittings on this or other models may reveal occasions when the non-linear method is advantageous.

5. CONCLUSIONS AND FURTHER WORK

In the study of many real dynamical systems arising in engineering, spatial discretizations such as finite differences or finite elements are more appropriate than Galerkin projection onto global basis functions. These spatial discretization methods do however have the drawback that they produce high-dimensional sets of ODEs from the original PDEs.

We have considered two methods for reducing the size of the dynamical system produced by a spatial discretization (finite difference in this case, but the method could just as easily be applied to other methods such as finite elements). In both cases the reduction in dimension is achieved by performing a two-level splitting in which "numerical mode shapes" determined from the structure of the linear parts of the large set of ODEs are used in an analogous way to mode shapes in the standard global Galerkin method. The ODEs are projected onto a small number of those modes which (linearly) contract the least and are therefore likely to be dynamically the most important. A further development of this two-level splitting, described in section 4.3, is to try to construct an approximate inertial manifold following closely the work on non-linear Galerkin methods.

Results show that the reduced dynamical systems produced by these new methods reproduce the main features (multiple solutions and the bifurcations between them) of the original system dynamics. (Here, strictly speaking, "original system" refers to the large set of ODEs produced by the original spatial discretization, rather than the PDEs, but this is not an issue fundamental to the methods presented). Dynamical systems with dimension low enough to be studied in great depth have thus been produced from systems of equations which are expensive to integrate even numerically. As such, these methods suggest an approach allowing detailed investigation of problems which are usually considered too large.

En route we have employed a number of techniques which, although standard in the mathematical and numerical analysis literature, have not been commonly used together in structural analysis: the use of the Rosenbrock method for integration of stiff equations; the use of singular value decomposition for inversion of the matrices arising from the finite difference scheme; the flat Galerkin projection of the fully non-linear equations onto a few numerical eigenvectors. The most distinctive innovation was the attempt to apply the

non-linear Galerkin method, using the techniques of inertial manifold approximation. However, although the method produced a low-dimensional model capturing the major features of the full non-linear dynamics, for the specific problem studied there appeared to be no significant advantage in using the fully non-linear Galerkin approach instead of a straightforward flat Galerkin projection onto the numerical eigenvectors. Determining whether use of the non-linear Galerkin approach is justified (i.e., whether an inertial manifold exists, and if so, of what dimension), is difficult in such problems. This, along with the extra effort involved in producing the corrected, non-linear Galerkin approximation, leads us to suspect that this extra step is perhaps unlikely to be widely useful in the study of non-linear elastodynamics.

ACKNOWLEDGMENTS

This work was supported by a grant from the EPSRC Nonlinear Mathematics Initiative. The authors are grateful to Dr A. A. Popov for detailed comments on the manuscript.

The authors are also grateful to Professor E. S. Titi for comments on the manuscript after it was accepted which suggest that the results presented here are not so much a failure of the non-linear Galerkin method but a success of the flat Galerkin method. A variety of configurations have since been suggested where the non-linear method and its variants may have a more beneficial impact and these are currently being investigated.

REFERENCES

1. P. Holmes and J. Marsden 1978 *Automatica* **14**, 367–384. Bifurcation to divergence and flutter in flow-induced oscillations: an infinite–dimensional analysis.
2. R. Baumgarten, E. Kreuzer and A. A. Popov 1997 *Nonlinear Dynamics* **12**, 307–317. A bifurcation analysis of the dynamics of a simplified shell model.
3. C. Foias, M. S. Jolly, I. G. Kevrekidis, G. R. Sell and E. S. Titi 1988 *Physics Letters A* **131**, 433–436. On the computation of inertial manifolds.
4. R. D. Russel, D. M. Sloan and M. R. Trummer 1993 *SIAM Journal of Scientific Computing* **14**, 19–43. Some numerical aspects of computing inertial manifolds.
5. H. G. Allen and P. S. Bulson 1980 *Background to Buckling*. Maidenhead, U.K.: McGraw-Hill.
6. G. H. Golub and C. F. van Loan 1989 *Matrix Computations*. Baltimore, MD: John Hopkins University Press.
7. W. H. Press, S. A. Teukolsky, W. T. Vetterling and B. P. Flannery 1992 *Numerical Recipes in C*. Cambridge: Cambridge University Press.
8. A. Debussche and M. Marion 1988 *Journal of Differential Equations* **100**, 173–201. On the construction of families of approximate inertial manifolds.